Enhanced photolysis in aerosols: evidence for important surface effects

Paul Nissenson,[a] Christopher J. H. Knox,[b] Barbara J. Finlayson-Pitts,[b] Leon F. Phillips*[c] and Donald Dabdub*[a]

Received 29th June 2006, Accepted 21st August 2006
First published as an Advance Article on the web 14th September 2006
DOI: 10.1039/b609219e

While there is increasing evidence for unique chemical reactions at interfaces, there are fewer data on photochemistry at liquid–vapor junctions. This paper reports a comparison of the photolysis of molybdenum hexacarbonyl, $Mo(CO)_6$, in 1-decene either as liquid droplets or in bulk-liquid solutions. $Mo(CO)_6$ photolysis is faster by at least three orders of magnitude in the aerosols than in bulk-liquids. Two possible sources of this enhancement are considered: (1) increased light intensity due to either Morphology-Dependent Resonances (MDRs) in the spherical aerosol particles and/or to increased pathlengths for light inside the droplet due to refraction, which are termed physical effects in this paper; and (2) interface effects such as an incomplete solvent-cage at the gas–liquid boundary and/or enhanced interfacial concentrations of $Mo(CO)_6$, which are termed chemical effects. Quantitative calculations of the first possibility were carried out in which the light intensity distribution in the droplets averaged over 215–360 nm was obtained for 1-decene droplets. Calculations show that the average increase in light intensity over the entire droplet is 106%, with an average increase of 51% at the interface. These increases are much smaller than the observed increase in the apparent photolysis rate of droplets compared to the bulk. Thus, chemical effects, *i.e.*, a decreased solvent-cage effect at the interface and/or enhancement in the surface concentration of $Mo(CO)_6$, are most likely responsible for the dramatic increase in the photolysis rate. Similar calculations were also carried out for broadband (290–600 nm) solar irradiation of water droplets, relevant to atmospheric conditions. These calculations show that, in agreement with previous calculations by Mayer and Madronich [B. Mayer and S. Madronich, *Atmos. Chem. Phys.*, 2004, **4**, 2241] MDRs produce only a moderate average intensity enhancement relative to the corresponding bulk-liquid slabs when averaged over a range of wavelengths characteristic of solar radiation at the Earth's surface. However, as in the case of $Mo(CO)_6$ in 1-decene, chemical effects may play a role in enhanced photochemistry at the aerosol–air interface for airborne particles.

1. Introduction

There is increasing evidence for unusual chemistry at the interface between gases and liquids. For example, the kinetics of the reaction of gaseous Cl_2 with aqueous bromide droplets[2] and of gaseous OH free radicals with deliquesced NaCl particles[3] both show that there is much more rapid chemistry occurring at the gas–liquid interface than expected from the known bulk chemistry. This has significant implications not only for fundamental chemistry but also for reactions in the atmosphere, for example,[4,5] where the presence of particles with larger surface-to-volume ratios tends to favor such chemistry. Part of this unique chemistry is due to enhanced concentrations of the ions at the surface.[6–14]

An even newer area is that of photochemistry at interfaces. There is limited experimental[15,16] and theoretical[17–19] evidence that photolysis is more efficient at the interface. This has generally been attributed to decreased solvent-cage effects and hence decreased recombination of the photofragments, increasing the overall photolysis quantum yields. Given recent experimental and theoretical studies showing enhancement of certain involatile solutes[6–14] and gases[20,21,22] at the interface, a contribution due to enhanced surface concentrations is also possible. We refer to these two effects, decreased solvent-cage and concentration enhancement, as chemical effects on the photochemistry.

However, in the case of small liquid particles, there may also be contributions due to the fact that they are spherical, which gives rise to increased light intensity from two phenomena. The first is an enhanced light intensity at the surface due to Morphology-Dependent Resonances, MDR.[23–29] The second is a net increase in light intensity in the droplet as a whole due to increased path lengths in the particles arising from refraction as the light beam crosses the air–liquid interface.[1,30–32] We refer to these effects as physical effects on the photochemistry.

We report here a dramatic increase in the photolysis rate of $Mo(CO)_6$ dissolved in 1-decene for small droplets ($\sim$2 μm

[a] *Department of Mechanical and Aerospace Engineering, University of California, Irvine, California 92697-3975, USA. E-mail: ddabdub@uci.edu; Fax: +1-949-824-8585; Tel: +1-949-824-6126*
[b] *Department of Chemistry, University of California, Irvine, California 92697-2025, USA*
[c] *Department of Chemistry, University of Canterbury, Christchurch, 8020, New Zealand. E-mail: leon.phillips@canterbury.ac.nz; Fax: +64-3-364-2110; Tel: +64-3-364-2425*

diameter) compared to the bulk solution from which they were generated. To the best of our knowledge, this is the first such observation of large differences in photolysis rates for particles compared to the bulk. It is of particular interest to separate the chemical effects, *i.e.* surface concentration enhancements and/or solvent-cage effects, from the physical effects of enhanced light intensity due to MDRs and/or refraction.

In this paper, we distinguish chemical from physical effects that contribute to the dramatic increase in photolysis using the following approach. First, calculations of the potential increase in light intensity due to MDRs and the refraction effect are performed. These calculations were carried out for droplets of pure 1-decene of the same size as those in the experiments. While one could in principle include the presence of the light-absorbing $Mo(CO)_6$ in the calculations to more closely mimic the experiments, this is complicated by the rapidly (few seconds) decreasing concentration of $Mo(CO)_6$ that was observed experimentally. In addition, Ruggaber *et al.*[31] showed that the presence of absorbing species in the droplets led to smaller light intensity enhancements from these physical effects than was the case for transparent particles. Thus, our calculations for droplets of the 1-decene solvent give an upper limit for the impact of MDRs and refraction in the experiments, which is the most relevant quantity for separating chemical from physical effects.

Second, the increased light intensity inside droplets due to broadband, rather than monochromatic, radiation striking a particle of known diameter is calculated. Previous treatments[1,23–32] of the physical effects reported light intensity enhancements for combinations of particular wavelengths and particle diameters but not for simultaneous irradiation of a given particle size over a range of wavelengths. This is important not only for interpretation of the experiments where a broadband Xe lamp was used as the light source, but also for application to atmospheric systems where airborne particles are irradiated by solar radiation, which is approximated by a blackbody at 6000 K, with a cutoff of 290 nm at the Earth's surface.[33]

By comparison of the experimental results to the calculated upper limit for physical effects of broadband radiation, it is shown that the chemical effects must predominate for $Mo(CO)_6$ photolysis.

Finally, we also carry out calculations for irradiation of water droplets, which are more representative of airborne particles than the $Mo(CO)_6$ system, by broadband radiation characteristic of the solar spectrum at the Earth's surface. The results are consistent with previous calculations with single wavelength–particle size combinations.[1] Again, these are upper limit calculations because the potential for light absorption by dissolved species is not included. Indeed, given the complexity of the composition of atmospheric aerosols, it would be difficult to include with confidence the variety of light absorbers and range of concentrations that are representative of the atmosphere. However, these calculations serve to illustrate the upper limit to increased light intensity (*i.e.*, physical effects), and hence enhanced photolysis rates, that can be expected by broadband solar irradiation of airborne droplets.

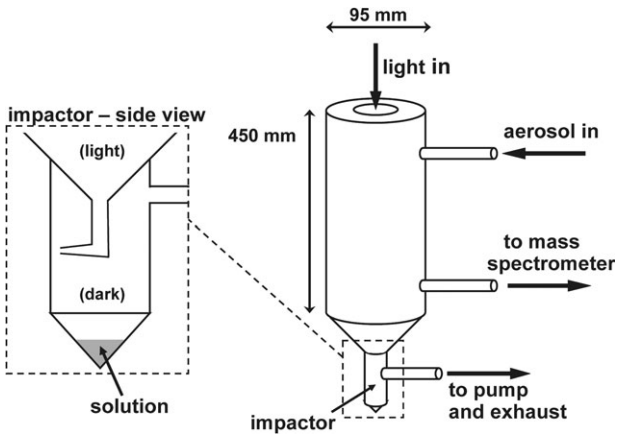

Fig. 1 Schematic of the stainless-steel photolysis system. Aerosols are introduced near the top of the chamber and are irradiated by a 450 Watt high-pressure xenon lamp as they travel toward the impactor. Once in the impactor, the aerosols condense and the resulting solution is shielded from the lamp's radiation.

2. Experimental and theoretical

2.1. Experimental

The aerosol experiments were conducted in a custom-built photolysis system, shown in Fig. 1. The irradiation section of the chamber was constructed from an internally-polished Stainless-steel tube. Light from an Osram-Sylvania XBO 450 Watt high-pressure xenon lamp passed through a water filter to remove infrared radiation, which causes heating, and then through a quartz window at the top of the chamber. Fig. 2 shows the relative intensity of the lamp in the region of interest based on data provided by the manufacturer. Aerosols were introduced through an aperture near the top of the chamber and with the flow in the direction of light propagation. A TSI model 3032 diaphragm pump drew gases through the system at a pressure slightly below one atmosphere. The range of gas

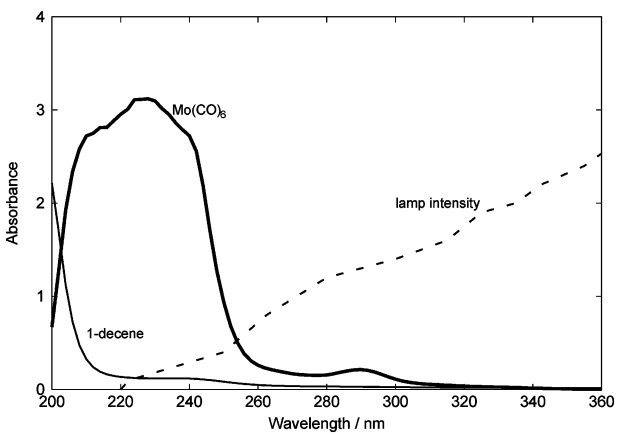

Fig. 2 UV absorption spectra (1 cm pathlength) of 1-decene, 10 μm $Mo(CO)_6$ in 1-decene with the solvent contribution subtracted out, and the relative lamp intensity from a manufacturer's spectrum. The structure on the lamp intensity is likely a result of the procedure used to digitize the spectral curve. The spectrum of $Mo(CO)_6$ is in good agreement with that reported in the literature.[64]

flows was such that the aerosol remained in the chamber for between 30 and 60 s before being deposited in an impactor located at the base of the chamber. The aerosols on the impactor were shielded from the light source so that no further photolysis could occur. Stainless-steel was used throughout the chamber and copper was used for the gas flow lines.

Aerosol droplets were produced by nebulizing solutions of molybdenum hexacarbonyl in 1-decene in a stainless-steel nebulizer. The $Mo(CO)_6$ was of stated 99% purity and the 1-decene was distilled under argon. The solutions were prepared by adding a known amount of $Mo(CO)_6$ to a fixed volume of 1-decene, sufficient to give a final concentration of 1 mM, and leaving the mixture under an argon atmosphere to dissolve overnight. Before each aerosol experiment, the infrared spectrum of the solution was measured using a Shimadzu Fourier Transform InfraRed (FTIR) spectrometer with an Attenuated Total Reflectance (ATR) attachment. The solution was then placed in the nebulizer and the chamber flushed with argon. Once the mass spectrum (obtained with an MKS PPT quadrupole residual gas analyser) indicated the absence of oxygen, the gas flow was switched to the nebulizer. The gas flow rate was 4 L min^{-1} and the solution was nebulized at a rate of 1 mL min^{-1}. The nebulizer typically produced a log-normal aerosol size distribution with a median diameter of 2 μm, as determined with a TSI model 3321 aerodynamic particle sizer. Once the aerosol flow was stable, the high-pressure xenon lamp was switched on. The aerosol passed through the chamber and a sample comprising all but the smallest droplets (diameter $\leq$300 nm) was collected as a liquid at the bottom of the impactor (Fig. 1). The collected liquid was shielded from the light. The liquid (several mLs were collected per experiment) was then transferred to the ATR crystal using a pasteur pipette and was analyzed using ATR-FTIR. Control experiments were carried out in which aerosols were passed through the chamber in the dark and collected in the same way as in the photolysis experiments. No loss of $Mo(CO)_6$ was observed in these blank experiments.

The bulk-liquid photolysis experiments were conducted outside the chamber. A 2 cm × 2 cm × 2 cm quartz cuvette was filled with $Mo(CO)_6$ in 1-decene solution. The cuvette was then flushed with argon and sealed under an argon atmosphere. The cuvette was irradiated using the same xenon lamp, at the same average distance from the lamp as in the aerosol experiments, so that the average-light intensities in the aerosol and bulk-liquid experiments were comparable. The size of the light beam was such that the entire contents of the cuvette were irradiated. After irradiation, samples were withdrawn for ATR-FTIR analysis.

2.2. Calculation of the light intensity distribution in droplets

To calculate an upper limit for the physical effects of increased light intensity, we carried out calculations of the maximum increases in average light intensity that were possible for broadband irradiation of droplets of the pure solvent; the presence of an absorber such as $Mo(CO)_6$ will dampen the light intensity enhancement,[31] so these calculations represent an upper limit for the physical effects in the experiments. For these calculations, the average light intensity distribution within a droplet of 1-decene was calculated (as described in Section 2.2.1) relative to a bulk-liquid slab when both are irradiated by light with the spectral distribution shown in Fig. 2. The average relative intensity at the interface is of particular interest and was calculated because the surface area-to-volume ratio is much greater in the aerosol phase than in the bulk-liquid phase, and the solvent-cage effect is also expected to be greatly reduced in that region. The calculations presented here apply to spherical liquid aerosols. Treatment of solid particles is beyond the scope of this paper.

2.2.1 Light intensity distribution for a single wavelength. The numerical model applied in this study utilizes the wave description of light, because the droplet diameter ($\sim$2 μm) is similar to the wavelength of the incident light ($\sim$0.5 μm). In the model, a polarized plane-wave travelling in the $+z$ direction through a gas is incident upon an isotropic and homogeneous spherical droplet (Fig. 3). The equations for a time-harmonic electromagnetic field (**E**, **H**) in such a droplet are derived from Mie theory and are found in the literature.[26,27] Two parameters determine the intensity distribution within the droplet: (1) The size parameter, $x = (2\pi a)\,\lambda^{-1}$, where a is the droplet radius and λ is the incident wavelength; (2) the index of refraction ratio between the solution and gas, m, which is a function of wavelength. All light intensities were calculated with code based in part on that developed by Barber and Hill.[27]

The intensity at any point within the droplet relative to the incident intensity is given by eqn (1),[26,27]

$$I^{\mathrm{drop}}(m,\lambda,r/a,\Theta,\Phi) = \frac{m\,\mathbf{E}(m,\lambda,r/a,\Theta,\Phi)\cdot\mathbf{E}^{*}(m,\lambda,r/a,\Theta,\Phi)}{(E_0)^2}, \quad (1)$$

where r, Θ, Φ are spherical coordinates, $(E_0)^2$ is the incident intensity and $\mathbf{E}^*$ is the complex conjugate of the electric field. I^{drop} is a function of λ (not x) in eqn (1) because the intensity distribution is calculated for a droplet of fixed radius. (The term 'wavelength' is favored over the term 'size parameter' in this paper for this reason.) As in the work of Barber and Hill,[27] the electric field is expressed as an infinite series of vector spherical harmonics. Enough terms of the series are summed over until convergence is reached. I^{drop} is then calculated from the electric fields.

The intensity within a bulk-liquid slab of a non-absorbing liquid relative to the incident intensity is given by the

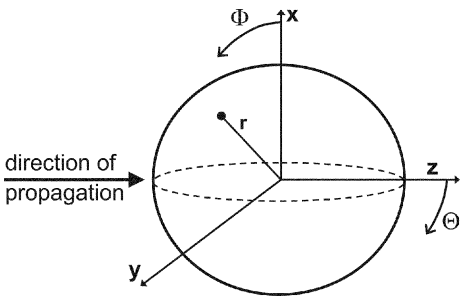

Fig. 3 Coordinate system used in this paper. Both Cartesian (x, y, z) and spherical (r, Θ, Φ) coordinates are shown.

transmission coefficient (T),[34]

$$T = \frac{4m_{r,0}m_{r,slab}}{(m_{r,0} + m_{r,slab})^2}, \quad (2)$$

where $m_{r,0}$ is the real part of the index of refraction of the gas and $m_{r,slab}$ is the real part of the index of refraction of the bulk-liquid. Note that since $m_r \approx 1.44$ for 1-decene over the range 215–360 nm,[35] $T \approx 1$ and the intensity in the bulk-liquid slab is similar to the incident intensity for both solvents.

For direct comparison to the experimental results, the quantity of interest is not the absolute intensity within the droplet or the bulk-liquid slab, but rather the ratio between these two values. This *relative intensity* quantifies the intensity enhancement within a droplet compared to a bulk-liquid slab, due to the droplet's spherical shape. The relative intensity is defined as,

$$I^{rel}(m,\lambda,r/a,\Theta,\Phi) \equiv \frac{I^{drop}(m,\lambda,r/a,\Theta,\Phi)}{T}. \quad (3)$$

If $I^{rel}(m, \lambda, r/a, \Theta, \Phi)$ is greater than unity, there is an intensity enhancement at that point in the droplet relative to the bulk-liquid slab caused solely by the droplet's spherical shape. Note that since the transmission coefficient is approximately unity, eqn (3) also gives a close approximation of the intensity enhancement in a droplet relative to the incident intensity.

2.2.2 Light intensity distribution for broadband radiation (multiple wavelengths). In the experiments, 1-decene droplets were irradiated by broadband light from a xenon lamp. As seen in Fig. 2, $Mo(CO)_6$ absorbs light in the 200–360 nm region and the overlap with the lamp emission is in the 215–360 nm range. The solvent, 1-decene, has a weak absorption below 250 nm, rising below 210 nm. As discussed earlier, for simplicity we calculate the increase in intensity in the droplets due to physical effects (MDRs and refraction) using droplets of pure 1-decene.

The 1-decene solvent initially contained the light absorber $Mo(CO)_6$, whose concentration rapidly dropped to undetectable levels in less than a minute. As discussed by Ruggaber *et al.*,[31] the presence of absorbing compounds in the droplets decreases the number and size of the MDR peaks, as well as the overall light enhancement in the particles. For example, they calculated that the overall enhancement of light intensity decreased from a factor of 2.34 for pure water droplets with a radius of 1 μm to a factor of 1.57 for the case of a pure aerosol particle for which the imaginary part of the index of refraction was 10^{-2}. The calculations presented here will therefore slightly overestimate the light intensity enhancement. However, this only strengthens the ultimate conclusion that it is not the light intensity enhancement but the solvent-cage effects at the interface that play the major role in the experimentally observed fast photolysis of the droplets compared to the bulk solution.

In the numerical model, the real part of the index of refraction for 1-decene (m_r) is interpolated from data measured by Forziati *et al.*[35] The imaginary part of the index of refraction (m_i) is set to 5.4×10^{-7} from 215–250 nm based on the absorption coefficient calculated[36] using the spectrum in Fig. 2, 1.0×10^{-8} from 270–360 nm (*i.e.*, negligible absorption in this region) and linearly interpolated between those two values in the 250–270 nm range.

We find that the range of wavelengths used in the calculations, the type of incident intensity (lamp spectrum from the experiment, blackbody spectrum, *etc.*) and the droplet size do not affect the distribution of light inside the droplets significantly provided that the wavelength range includes at least a few MDRs, the wavelength intervals are small enough to give a true average of the relative intensity over the MDRs, the intensity of the radiation is a smoothly changing function of λ and the size parameter range is within the Mie theory range ($x \sim 5$–100).[24,37] Simulations were run with progressively smaller wavelength intervals until convergence was reached to ensure that the resonances were completely averaged over.

The radiation falling on droplets in the experiment and in the troposphere is non-uniform over direction. Therefore, a useful quantity is the angle- and wavelength-averaged intensity distribution as a function of normalized radius, since it is independent of the direction of illumination. The equation for this distribution is derived by integrating $I^{rel}(m, \lambda, r/a, \Theta, \Phi)$ over Θ and Φ,[27]

$$I^{rel}_{ang}(m,\lambda,r/a) = \frac{\frac{1}{4\pi}\int_0^{2\pi}\int_0^{\pi} m\mathbf{E}\cdot\mathbf{E}^*\sin\Theta\, d\Theta\, d\Phi}{(E_0)^2 T}, \quad (4)$$

where the subscript 'ang' refers to the angle-averaged relative intensity. At each radial shell, $I^{rel}_{ang}(m, \lambda, r/a)$ is calculated for every wavelength. Averaging over all wavelengths yields the angle- and wavelength-averaged intensity distribution as a function of normalized radius, $I^{rel}_{\lambda,ang}(r/a)$.

$I^{rel}_{\lambda,ang}(r/a)$ provides the average relative intensity at different spherical shells within the droplet; $I^{rel}_{\lambda,ang}(r/a = 1)$ is the average relative intensity at the gas–liquid interface. In calculating $I^{rel}_{\lambda,ang}(r/a)$, the droplets are taken to be spherically-symmetrical since they are liquids, and each plane wave may be treated independently. Calculations in Appendix A show that there is a low probability of plane-wave interaction within the droplets in the experiment, which justifies the latter assumption. Therefore, $I^{rel}_{\lambda,ang}(r/a)$ will be the same for any irradiation scenario. In this paper, $I^{rel}_{\lambda,ang}(r/a)$ is calculated for a droplet illuminated from only one direction with perpendicularly polarized plane-waves. The results obtained for this scenario are the same for a droplet illuminated from many directions by plane-waves of varied polarizations, as in the experiment.

We have also examined the average relative intensity over the cross section of a droplet illuminated by a spectrum of plane-waves from one direction. Although these results only apply to this specific type of illumination, they are useful in understanding the intensity distribution for the general cases. In order to calculate the intensity over the droplet cross section, the droplet is divided by a Cartesian-coordinate grid. At each gridpoint, the relative intensity is calculated for each wavelength. Averaging over all wavelengths gives $I^{rel}_{\lambda}(r/a, \Theta, \Phi)$. The average relative intensity throughout the entire droplet is calculated by averaging $I^{rel}_{\lambda}(r/a, \Theta, \Phi)$ over all points in the droplet.

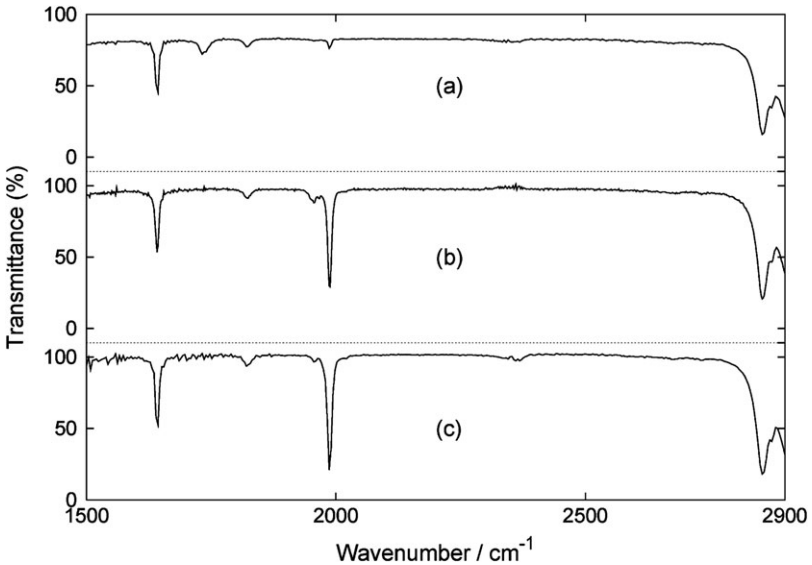

Fig. 4 Infrared absorption spectra of a) $Mo(CO)_6$ in 1-decene irradiated for 30 s in the aerosol phase, (b) $Mo(CO)_6$ in 1-decene irradiated for one hour in the bulk-liquid phase, (c) non-irradiated $Mo(CO)_6$ in 1-decene. The only feature that changes significantly is the ν(CO) stretch at 1987 cm^{-1}.

3. Results and discussion

3.1. Experimental results

Fig. 4 shows the ATR-FTIR spectra from 1500–2900 cm^{-1} for $Mo(CO)_6$ in 1-decene before and after irradiation for both aerosols and the bulk-liquid solution. The only feature in the spectrum that shows a significant change is the carbonyl stretch at 1987 cm^{-1}. In the bulk-liquid phase spectrum, no significant change is observed at 1987 cm^{-1} after one hour of irradiation whereas, in sharp contrast, this peak is almost completely absent from the aerosol spectrum after only $\sim$30 seconds of irradiation. The magnitude of the change in intensity of the carbonyl peak can best be compared to that of the bulk solution by reference to a solvent peak. Using the C–H stretch at 2925 cm^{-1} as the reference, the absorbance of the CO stretch at 1987 cm^{-1} in the droplets irradiated for 30 s decreased by about a factor of 14 relative to that in the bulk irradiated for one hour. It is important to note that the passage of the solution through the aerosol system with the light turned off produced less than a 10% change in the 1987 cm^{-1} peak. This rules out changes in the aerosol sample due to impaction, *e.g.* volatilization of $Mo(CO)_6$ into the gas phase.

Another possible source of loss of $Mo(CO)_6$ in the aerosols is the heating of particles during irradiation. The vapor pressures of solid $Mo(CO)_6$ and liquid 1-decene at room temperature are $\sim$10 Torr and 1.6 Torr, respectively, so that heating could, in principle, preferentially evaporate $Mo(CO)_6$. A calculation of the upper limit for the heating of the droplets, however, shows that this cannot cause the observed loss of $Mo(CO)_6$ from the aerosol. For example, absorption of light at 255 nm, mid-range in the photochemically active wavelength region (Fig. 2), of a number of photons equal to the number of $Mo(CO)_6$ molecules in the droplet corresponds to 2.0×10^{-12} J of energy. The bond dissociation energy for dissociation of the first CO from $Mo(CO)_6$ is 167 kJ mol^{-1},[38] so that the first dissociation step will take up 7.0×10^{-13} J in each droplet. The net energy left for heating the droplet is 1.3×10^{-12} J. Using the known heat capacity at constant pressure of 1-decene (71.8 cal mol^{-1} K^{-1});[39] and its density (0.74 g cm^{-3}), a temperature increase of 0.2 °C is calculated. As this assumes a closed system with no heat exchange with the surrounding gases, it represents an upper limit. This is unlikely to be sufficient to cause the loss of most of the $Mo(CO)_6$ from the droplets in 30 s, as was observed in the experiment (Fig. 4).

In short, there is a large difference between the photolysis rates of $Mo(CO)_6$ in the bulk-liquid and aerosol phases that is not due to volatilization by heating or impaction. The metal walls of the aerosol photochemistry chamber are more highly reflecting than those of the quartz cuvette used to irradiate the bulk solution; however, this is very unlikely to increase the light intensity by the orders of magnitude needed to explain the aerosol experiment, particularly since the light beam was directed along the vertical axis of the reactor. From the factor of 14 change in the carbonyl stretch (Fig. 4), and taking into account the ratio of exposure times (a factor of 120), we calculate a lower limit of at least three orders of magnitude for the ratio of the aerosol photolysis rate to the photolysis rate for bulk $Mo(CO)_6$ solutions.

A small peak at $\sim$1730 cm^{-1} appeared in Fig. 4a, suggesting the formation of new products such as carbonyls in the aerosol. However, the formation of a similar peak has been observed when 1-decene alone is nebulised in room light, suggesting that some oxidation of either the solvent or an impurity within it is responsible for this peak. There were no significant changes in the spectrum unique to $Mo(CO)_6$ below 1500 cm^{-1}. There is visual evidence suggesting that the $Mo(CO)_6$ decomposed into molybdenum and carbon monoxide, and the mass spectrometer often indicated that the amount of carbon monoxide in the chamber increased during irradiation. (This observation was not always reproducible

because the mass spectrometer was operating at the limit of its sensitivity.)

The photochemistry of transition metal hexacarbonyls has been reviewed by Wrighton.[40] The photolysis initially involves the loss of one CO and the formation of $Mo(CO)_5$, which can fragment with further loss of CO if it retains sufficient energy;

$$Mo(CO)_6 + h\nu \rightarrow Mo(CO)_5^* + CO \quad (1)$$

$$Mo(CO)_5^* \rightarrow Mo(CO)_4 + CO \quad (2)$$

As discussed by Wrighton,[40] if there is a ligand that can react with the $Mo(CO)_5$ fragment in the solution phase,

$$Mo(CO)_5 + L \rightarrow Mo(CO)_5L \quad (3)$$

recombination of the $Mo(CO)_5$ with CO,

$$Mo(CO)_5 + CO \rightarrow Mo(CO)_6 \quad (4)$$

is effectively quenched and the photolysis quantum yield is unity. For example, Lian *et al.*[41] carried out femtosecond infrared studies of the dissociation and geminate recombination of $M(CO)_6$ for M = Cr, W and Mo in heptane solution. The primary process yielded $M(CO)_5$ + CO, where the $M(CO)_5$ was vibrationally excited, and geminate recombination on a timescale faster than 300 fs resulted in the formation of vibrationally hot $M(CO)_6$. The fraction of fast geminate recombination (about 6% for M = Mo) was consistent with literature values for photo-substitution quantum yields when allowance was made for vibrational relaxation of the vibrationally hot species. Vaida and coworkers[42] studied the photolysis of $Cr(CO)_6$ on a picosecond timescale in the gas phase and in solutions of methanol, benzene or cyclohexane, respectively. They observed the loss of one CO to form $Cr(CO)_5$ within the first 25 ps of photolysis in solution, whereas in the gas phase the loss of up to four CO groups at a time was observed. While they did not find evidence for recombination of $Cr(CO)_5$ with CO in solution, in our studies of $Mo(CO)_6$ in bulk solution there was no other reactant present, so the only reaction channel available to the $Mo(CO)_5$ would have been diffusion-limited recombination with CO, a process which would have been too slow to be observed in the experiments of Lian *et al.*[41] and Vaida and coworkers.[42] A unit quantum yield is generally assumed to be true in the gas phase,[40] where there is no solvent-cage to hold the fragments of reaction (1) together.[43,44]

The results of our aerosol studies show that much of the CO produced in the primary process escaped, similar to the situation in the gas phase. Any re-formed $Mo(CO)_6$ would have been subject to photolysis again, and the $Mo(CO)_5$ and smaller fragments would themselves have been photolysed during the 30–60 s passage through the photolysis vessel.

3.2. Calculation of the upper limit for physical effects of increased light intensity in droplets

As discussed earlier, the sources of enhanced photochemistry in aerosols compared to bulk-liquids are either chemical or physical (*i.e.* light intensity) effects. Physical effects include enhanced light intensity in droplets due to MDRs and increased effective pathlengths for the light caused by refraction of the beam at the gas–liquid interface. MDRs are known to create intensities in a droplet that are orders of magnitude larger than in a bulk-liquid slab.[23–28] The relative intensity is a sensitive function of λ for a droplet of fixed radius. Most relevant to interpreting our experiments is the question of whether these resonances are diluted when they are averaged over an entire wavelength spectrum.

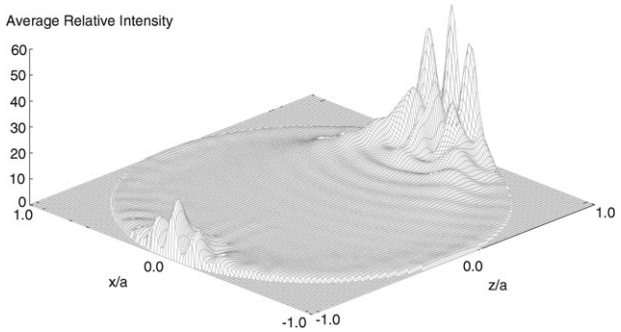

Fig. 5 I_λ^{rel} across a 1-decene droplet central cross section. Results shown are for droplets of radius a = 1 μm irradiated by a spectrum of perpendicularly-polarized (relative to the x–z plane) plane-waves (215–360 nm). The x- and z-axes are normalized to the droplet radius. The simulations use a resolution of 200 × 101 gridpoints. The average value of I_λ^{rel} over the 1-decene droplet cross section is 2.98 and the peak value is 59.3.

Fig. 5 shows the wavelength-averaged relative intensity distribution over the central cross section (*i.e.* for the equatorial cross section corresponding to y = 0.0 μm) of a 1-decene droplet of radius a = 1 μm. The droplets are irradiated from one direction by perpendicularly-polarized plane-waves over the wavelength range λ = 215–360 nm, corresponding to a size parameter range x = 17.5–29.2. The average value of I^{rel} is 2.98 over the 1-decene central cross section with a peak value of 59.3. The average value of I^{rel} over the entire 1-decene droplet is 2.06.

Fig. 6 shows the angle- and wavelength-averaged relative intensity distribution, $I_\lambda^{rel}(r/a)$, as a function of r/a for a 1-decene droplet in the experiment (the water data shown in the figure are discussed below). There is a significant intensity enhancement (an average factor of 2.06) throughout most of the droplet, including at the interface (r/a = 1 μm) where the average relative intensity is 1.51. Although the illumination conditions for this calculation are the same as those used to produce the results in Fig. 5, the results in Fig. 6 apply for illumination from any direction or combination of directions.

While the intensity enhancement at the droplet's circumference demonstrated in Fig. 5 may appear contradictory with the reduced enhancement at the droplet interface demonstrated in Fig. 6, these two figures are consistent; Fig. 5 only shows the equatorial cross section (y = 0.0 μm) of a droplet, while Fig. 6 accounts for the intensity over the entire droplet.

In the experiment, the particle size distribution is not monodisperse, in that the nebulizer produces a log-normal size distribution with a median diameter of 2 μm. Fig. 7 shows that the relative intensity at the interface for 1-decene droplets of various sizes averaged over all angles and wavelengths, $I_{\lambda,ang}^{rel}(r/a)$, is greater than unity over a wide range of diameters, ~1–5 μm. At smaller droplet diameters, $I_{\lambda,ang}^{rel}(r/a)$ decreases rapidly as Mie theory becomes less applicable because λ becomes much larger than the droplet size.

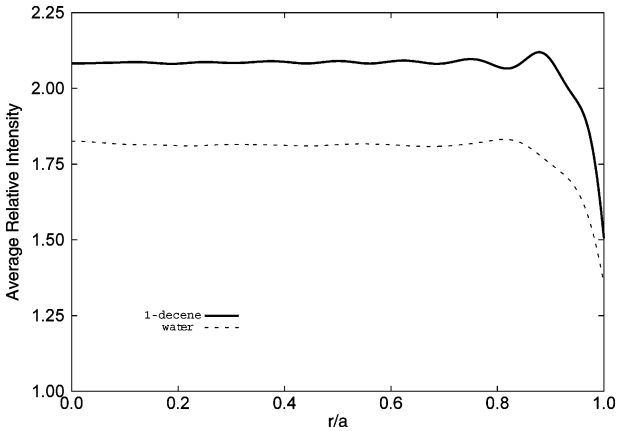

Fig. 6 The angle- and wavelength-averaged relative intensity distribution ($I^{rel}_{\lambda,ang}$) as a function of the normalized distance from the droplet center for a 1-decene droplet and for a water droplet. Both droplets are 1 μm in radius and irradiated from one direction by perpendicularly-polarized (relative to the *x*–*z* plane) plane-waves. The 1-decene droplet is irradiated by the wavelength range λ = 215–360 nm. The water droplet is irradiated by the actinic flux (λ = 290–600 nm) corresponding to a 30° solar zenith angle and an average surface albedo that varied from 0.05 in the 290–400 nm region to 0.15 in the 660–700 nm region.[33] At the interface (r/a = 1), the average value of the intensity is 1.51 for 1-decene and 1.35 for water.

3.3. Chemical *versus* physical sources of enhanced photochemistry in droplets

Our calculations focused on the average enhancement in light intensity in droplets irradiated by broadband radiation. However, they are consistent with earlier work carried out for explicit combinations of wavelength and droplet radius[1,28–32,45] and show that enhanced light intensities in the particles cannot be responsible for the dramatic increase in the photolysis rate of $Mo(CO)_6$ observed in the experiments. Thus, on average there is a light intensity enhancement factor of 2.06 in 1-decene droplets compared to the bulk-liquid due to the MDR effects, with an enhancement factor of 1.51 at the interface. This is well below the estimated three orders of magnitude increase measured for the photolysis of the aerosols.

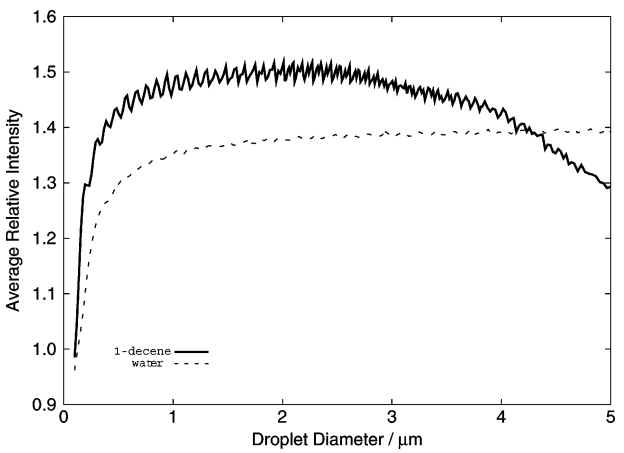

Fig. 7 The angle- and wavelength-averaged relative intensity distribution at the interface ($I^{rel}_{\lambda,ang}(r/a = 1)$) as a function of the droplet diameter. The droplets are irradiated under the same conditions as in Fig. 6, however, similar results are observed for any arbitrary broadband illumination.

Given that the physical effects of enhanced light intensity cannot explain the experimental observations, in the absence of other reasonable explanations, this leaves chemical effects as the main source of the enhanced photochemistry. While we cannot rule out with certainty as yet unknown factors, such as a dramatic change in the absorption coefficients for $Mo(CO)_6$ at the surface compared to the bulk, there are few, if any, data in the literature supporting such effects. The first chemical effect is potential enhancement of the concentration of the reactant, $Mo(CO)_6$, at the interface. It is notable that the enhanced surface concentrations predicted for ionic species in water depend on the ions being highly polarizable,[6–12,17,46–54] which is likely to be the case for $Mo(CO)_6$ even in comparison with the relatively large solvent molecule 1-decene. The second interface effect is the increased quantum yields at the surface due to the absence of a complete solvent-cage. As discussed in the Introduction, solvents in bulk-liquids tend to encapsulate photo-fragments, leading to a higher probability of recombination (the solvent-cage effect) and a correspondingly lower quantum yield for decomposition. Thus, quantum yields can vary significantly with a molecule's position within a droplet. Fig. 8 is a schematic diagram of the change in the solvent-cage effect at the interface. In the simplest approach, one might think of half of the solvent-cage being absent. However, since the density of the solvent decreases at the interface, and is also quite anisotropic with respect to its distribution around solutes, the change in the solvent-cage effect on the quantum yield should be significantly greater than a factor of two.

There is some experimental evidence to support this. For example, Graham *et al.*[15] studied the photodissociation of OClO in thin films and adsorbed on ice; they reported the production of ClO in the gas phase with a translational temperature of 1721 K, indicating direct ejection of this photofragment from the surface. Similarly, Furlan[16] measured hyperthermal iodine atoms at a translational temperature of 480 K desorbing from the surface when 4-iodobenzoic acid in glycerol was photolyzed at 278 K; he attributed this to direct

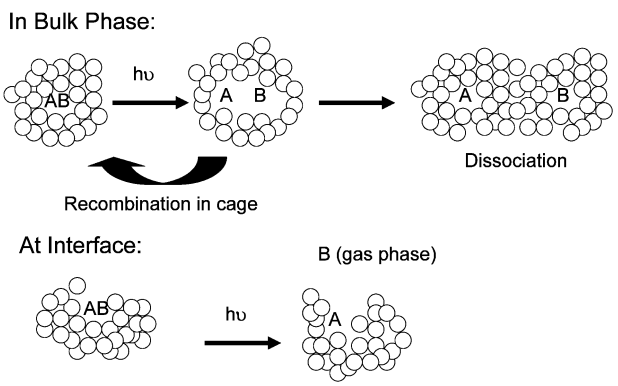

Fig. 8 Schematic diagram of decreased solvent-cage effects leading to increases in the overall quantum yields for dissociation at the interface compared to the bulk phase.

ejection of the iodine atoms generated by photolysis of molecules in the top 1 nm of the liquid.

Theoretical studies have also provided considerable insight into surface photochemistry and lead the available experimental data in many cases. For example, Benjamin and coworkers[18] used molecular dynamics simulations to predict that the photodissociation of OClO at the surface of liquids proceeds with essentially no recombination of the fragments in the solvent-cage, in contrast to photolysis in the bulk liquid where there is 60% recombination. Similarly, they predict that for photolysis of ICN in water, only 8% of the I and CN photofragments recombine in the topmost layer, compared to 85% in the bulk.[19]

When the $(2\ \mathrm{cm})^3$ bulk-liquid slab is nebulized into droplets roughly 2 μm in diameter, its surface area increases by approximately five orders of magnitude. This increased surface area is expected to produce higher quantum yields for $Mo(CO)_6$ photolysis in the aerosol phase than in the bulk-liquid phase, to a maximum extent that is given by the ratio of the quantum yield in the gas-phase to the quantum yield in solution. As the $Mo(CO)_6$ is lost at the surface, it can be readily replaced. For example, for a typical diffusion coefficient in the liquid phase of $\sim 10^{-5}\ \mathrm{cm^2\ s^{-1}}$, diffusion from the center of the droplet to the surface will occur on a millisecond time scale, much shorter than the ~30 s residence time in the reactor. The chemical effects of a reduced solvent-cage and/or enhanced surface concentrations are therefore most likely to account for most of the observed difference in quantum yields of $Mo(CO)_6$ decomposition between the aerosol and the bulk-liquid phases. While future work should focus on studying the variation with solute concentration, wavelength and photolysis time, the studies reported here clearly establish the enhanced photochemistry occurring in aerosols compared to the bulk.

4. Atmospheric applications

The purpose of the calculations was to place an upper limit on the contribution of the physical effects (MDR and refraction path length effects) to the observed enhancement of photodecomposition of $Mo(CO)_6$ in 1-decene droplets compared to the bulk solution. However, it is also of interest to extend the calculations of the effects of broadband radiation to water droplets in the atmosphere. Over the range of relative humidities encountered in the troposphere, many particles are aqueous solutions.[33] Hence, we also carried out a series of calculations for water droplets, again choosing a diameter of 2 μm and broadband radiation characteristic of the earths' surface.

In the troposphere, water droplets are irradiated by the solar actinic flux. The water droplet simulations use values for the actinic flux at a solar zenith angle of 30° and an average surface albedo that varied from 0.05 in the 290–400 nm region to 0.15 in the 660–700 nm region.[33] If different actinic flux data were chosen, the results would not change significantly because, although the intensity magnitude in the droplet would change, the intensity relative to the bulk-liquid slab would not. In the troposphere, the wavelength range of interest—where photons are energetic enough to photolyze most relevant species—is $\lambda \sim 290$–600 nm. Data for the real part of the index of refraction of water as a function of wavelength are obtained from ref. 55 and 56. The imaginary part of the index of refraction is set to 10^{-8}, which is the maximum value for water over 290–600 nm.[55,56]

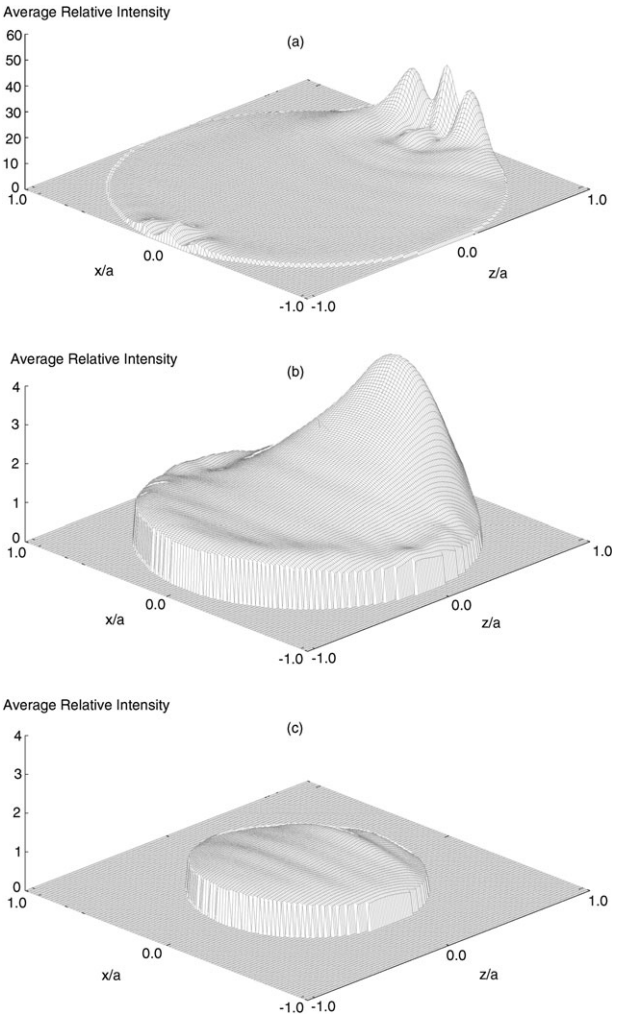

Fig. 9 I_λ^{rel} across a water droplet cross section at (a) $y = 0.0$ μm, (b) $y = 0.50$ μm and (c) $y = 0.80$ μm. Results shown are for droplets of radius $a = 1$ μm irradiated by a spectrum of perpendicularly-polarized (relative to the x–z plane) plane-waves over $\lambda = 290$–600 nm. The x- and z-axes are normalized to the droplet radius. The simulations use a resolution of 200 × 101 gridpoints. These water droplets are irradiated by the actinic flux corresponding to a solar zenith angle of 30° and an average surface albedo that varied from 0.05 in the 290–400 nm region to 0.15 in the 660–700 nm region.[33] The average values of I_λ^{rel} over the water droplet cross sections are 2.24, 1.51 and 0.91 for (a), (b) and (c), respectively. The peak values of I_λ^{rel} over the water droplet cross sections are 27.0, 3.90 and 1.16 for (a), (b) and (c), respectively.

Fig. 9 shows the wavelength-averaged relative intensity distribution over the central cross section corresponding to $y = 0$ μm (Fig. 9a), as well as for cross sections at $y = 0.50$ μm (Fig. 9b) and at $y = 0.80$ μm (Fig. 9c). The intensity clearly falls off rapidly for cross sections away from $y = 0$ μm. At this central cross section, the average value of the relative intensity is 2.24, but falls to 1.51 and 0.91 for $y = 0.50$ μm and $y = 0.80$ μm, respectively.

Fig. 6 shows the angle- and wavelength-averaged relative intensity distribution as a function of the normalized distance from the droplet center (r/a) for water droplets irradiated over the 290–600 nm range. Fig. 7 shows similar data for the interface intensity. As for the 1-decene droplets, there is a significant intensity enhancement throughout the droplet, including at the interface. The intensity enhancement is different in the water droplet compared to the 1-decene droplet due to the two solutes having different indices of refraction.

The values presented here for I^{rel} averaged over the entire water droplet are in good agreement with the values calculated by Mayer and Madronich.[1] For a water droplet of radius a = 1 μm, Mayer and Madronich calculated that the average value of the intensity enhancement throughout the droplet over 300–600 nm is ~1.76. Our value for the average relative intensity over the same range also yields 1.76.

In the atmosphere, aqueous aerosol particles will contain a number of solutes, some of which absorb light in the actinic region (*e.g.*, nitrate ions). Because the presence of absorbing compounds lowers the intensity enhancement,[31] the calculations presented here for water represent an upper limit to the light intensity enhancement throughout the droplet and at the interface for broadband irradiation of the particles by sunlight.

Quantum yields for photolysis of various species in solution are often smaller than those for the corresponding gas phase process. This is due to solvent-cage effects that keep the fragments formed on dissociation in close proximity, and hence increase the probability of the fragments recombining. However, if the solvent-cage effect is significantly decreased at the interface, the overall quantum yields will be larger than is the case in bulk-liquid solution. In this case, the production of free radicals and other reactive species could be enhanced at the surfaces of particles and clouds in the atmosphere, and also in thin liquid films on the surface of large objects such as buildings, leading to more active oxidation than is currently included in models. Potentially compounding this effect is the predicted concentration enhancement of a number of species, both neutral molecules and ions, at the air–water interface. For example, the concentrations of O_3 and H_2O_2, both sources of OH in the atmosphere, are predicted to be enhanced at the interface by factors of ~10 and 2, respectively, compared to the bulk.[21]

Similarly, a number of ions[6–8] have a propensity for the air–water interface. Quantum yields for the photolysis of ions in bulk aqueous solution are typically quite small, possibly due to a particularly strong solvent-cage effect for strongly solvated ions. This suggests that enhanced surface photochemistry, similar to that we observed for $Mo(CO)_6$, could be particularly important in such cases. One example of atmospheric interest is the nitrate ion. While initial calculations on the nitrate ion at infinite dilution[57] suggested it had a propensity for the surface, more recent studies at finite concentration[58] indicate that the ion tends to remain below the surface. However, this may still be sufficiently close to the interface that a full solvent shell is not active and some of the enhancement in surface photochemistry seen in the present studies could potentially occur.

Nitrate ions decompose by two paths:[59–61]

$$NO_3^- + h\nu \rightarrow NO_2 + O^- \quad (5)$$

$$NO_3^- + h\nu \rightarrow NO_2^- + O \quad (6)$$

Since O^- reacts with water to generate OH, both of these paths generate species that can, for example, oxidize organic molecules. If the quantum yields for ion photolysis are increased in the interfacial region, there is potential for enhanced oxidation of organics at aerosol interfaces compared to that expected due to O and OH generation from bulk photochemistry alone.

Molecular dynamics simulations[62] of nitrate ions in a 1 M solution do indeed suggest that the nitrate is less solvated close to the interface compared to the bulk. For example, on average there are about 8 water oxygen atoms within 4 Å of the nitrate N in the bulk, but only 6 water oxygens in the case of nitrate near the interface (defined as being within 8 Å of the surface).

Based on literature values of absorption coefficients, quantum yields and estimated concentrations in the aqueous phase in the atmosphere, Ruggaber *et al.*[31] suggest that the photolysis of $[Fe^{III}(OH)]^{2+}$ and $[Fe^{III}(OH)_2]^+$ are the major sources of OH in the condensed phase. Whether changes in solvent-cage effects at the interface also play a role in this photochemistry is unknown, but of considerable interest as well.

5. Conclusions

Our experiments show that $Mo(CO)_6$ in a 1-decene solution photolyses under broadband radiation ~3 orders of magnitude faster in the aerosol phase than in the bulk-liquid phase. Two possible sources of this enhancement are increased light intensity in the droplets and unique interfacial characteristics and processes. Calculations of the light intensity increases for the broadband radiation used in the experiments show there is an average intensity enhancement factor of 2.06 within a 1-decene droplet compared to a 1-decene bulk-liquid slab, with a 1.51 average enhancement factor at the droplet interface. Therefore, increased light intensity does not play the major role in the greatly enhanced rate of $Mo(CO)_6$ photolysis observed experimentally. This suggests that chemical effects, *e.g.*, a decreased solvent-cage effect and/or enhanced concentrations at the interface, resulting in dramatically increased overall quantum yields, are the most likely cause. Similar results are calculated for water droplets that are more relevant to tropospheric conditions for broadband solar radiation; they experience an average intensity enhancement factor of 1.76 with a 1.35 average enhancement factor at the interface. If the surface enhancement of photolysis yields in aerosol droplets and/or liquid films is a general effect, this could have significant implications in other areas, particularly in atmospheric photochemistry.

7. Appendix A: Justification of treating photons independently

The following is an estimate of the probability of photon interaction within the 1-decene droplets in the experiment and within the water droplets in the troposphere. The results

depend strongly upon the size of the droplet and the magnitude of the incident intensity.

In both the troposphere and in the experiment, the water and 1-decene droplets are irradiated by an intensity no greater than 1000 W m^{-2}. For the purposes of this calculation, we assume a droplet of radius $a = 1$ μm is irradiated with solar energy of intensity $\Gamma = 1000$ W m^{-2} with the peak intensity at $\lambda \sim 500$ nm. The energy of each photon is $E = hc/\lambda = 4 \times 10^{-19}$ J $photon^{-1}$, where h is Planck's constant and c is the speed of light in a vacuum.

The photon flux F through the droplet of cross section σ ($= \pi a^2 = 3 \times 10^{-12}$ m^2) is $F = (\sigma\Gamma)/E = 10^{10}$ photon s^{-1}. If the photons pass straight through the droplet, the photon residence time within the droplet is $t = (2a)/(c/m_r) = 9 \times 10^{-15}$ s, where $m_r \sim 1.35$. Therefore, only one in every 10^4 photons interact, and each photon that enters the droplet can be treated individually. However, Zhang *et al.*[63] showed that photons undergoing resonance reside in droplets for ~ns timescales. Therefore, roughly one in every ten resonant photons interact. However, since the majority of photons do not resonate and every photon interaction is equally likely to cause constructive or destructive interference, the authors believe that photon interaction can safely be ignored for the purposes of this paper.

8. Appendix B: Glossary of mathematical symbols

All variables used in this paper are in mks units.

a: droplet radius.

c: speed of light in a vacuum.

E: energy of photon.

$\mathbf{E}$: electric field.

$(E_0)^2$: incident intensity.

F: photon flux through a droplet.

Γ: actinic flux.

h: Planck's constant.

$I^{drop}(m,\lambda,r/a,\Theta,\Phi)$: Intensity at a point in a droplet relative to the incident intensity for a given wavelength.

$I^{rel}(m,\lambda,r/a,\Theta,\Phi)$: Intensity at a point in the droplet relative to a bulk-liquid slab for a given wavelength.

$I^{rel}_{ang}(m,\lambda,r/a)$: Average intensity over a spherical shell at radius r/a in a droplet relative to a bulk-liquid slab, for a given wavelength.

$I^{rel}_{\lambda}(r/a,\Theta,\Phi)$: Average intensity at a point in a droplet relative to a bulk-liquid slab over a range of wavelengths.

$I^{rel}_{\lambda,ang}(r/a)$: Average intensity over a spherical shell at radius r/a in a droplet relative to a bulk-liquid slab, averaged over a range of wavelengths.

λ: wavelength of light.

m: index of refraction containing both real and imaginary parts.

m_i: imaginary part of the index of refraction.

m_r: real part of the index of refraction.

$m_{r,0}$: real part of the index of refraction of the gas outside the droplet or bulk-liquid.

$m_{r,slab}$: real part of the index of refraction of the bulk-liquid.

σ: cross-sectional area of a droplet.

r,Θ,Φ: spherical coordinates.

t: time.

T: transmission coefficient; intensity in a bulk-liquid slab relative to the incident intensity.

x: size parameter.

Acknowledgements

We thank Sasha Madronich, Gregory Benford and Jane Ganske for stimulating discussions, and Lisa Wingen, Mike Ezell, Jennie Thomas, Doug Tobias and several anonymous reviewers for helpful comments on the manuscript. This work was supported by the United States National Science Foundation Collaborative Research in Chemistry (#0209719) and Environmental Molecular Science Institute (#0431512).

References

1 B. Mayer and S. Madronich, *Atmos. Chem. Phys.*, 2004, **4**, 2241.
2 J. Hu, Q. Shi, P. Davidovits, D. R. Worsnop, M. S. Zahniser and C. E. Kolb, *J. Phys. Chem.*, 1995, **99**, 8768.
3 E. M. Knipping, M. J. Lakin, K. L. Foster, P. Jungwirth, D. J. Tobias, R. B. Gerber, D. Dabdub and B. J. Finlayson-Pitts, *Science*, 2000, **288**, 301–306.
4 B. J. Finlayson-Pitts and J. C. Hemminger, *J. Phys. Chem. A*, 2000, **104**, 11463.
5 Finlayson-Pitts, *Chem. Rev.*, 2003, **103**, 4801.
6 P. Jungwirth and D. J. Tobias, *J. Phys. Chem. B*, 2000, **104**, 7702.
7 P. Jungwirth and D. J. Tobias, *J. Phys. Chem. B*, 2001, **105**, 10468.
8 P. Jungwirth and D. J. Tobias, *J. Phys. Chem. B*, 2002, **106**, 6361.
9 P. B. Petersen, J. C. Johnson, K. P. Knutsen and R. J. Saykally, *Chem. Phys. Lett.*, 2004, **397**, 46.
10 P. B. Petersen and R. J. Saykally, *Chem. Phys. Lett.*, 2004, **397**, 51.
11 S. Ghosal, J. C. Hemminger, H. Bluhm, B. S. Mun, E. Hebenstreit, G. Ketteler, F. Ogletree, F. Requejo and M. Salmeron, *Science*, 2005, **307**, 563.
12 P. B. Petersen, R. J. Saykally, M. Mucha and P. Jungwirth, *J. Phys. Chem. B*, 2005, **109**, 10915.
13 O. Hoefft, A. Borodin, U. Kahnert, V. Kempter, L. X. Dang and P. Jungwirth, *J. Phys. Chem. B*, (in press).
14 P. Jungwirth and D. J. Tobias, *Chem. Rev.*, 2006, **106**, 1259.
15 J. D. Graham, J. T. Roberts, L. D. Anderson and V. H. Grassian, *J. Phys. Chem.*, 1996, **100**, 19551.
16 A. Furlan, *J. Phys. Chem. B*, 1999, **103**, 1550.
17 I. Benjamin, *J. Phys. Chem.*, 1991, **95**, 3698.
18 I. Chorny, J. Vieceli and I. Benjamin, *J. Phys. Chem. B*, 2003, **107**, 229.
19 N. Winter and I. Benjamin, *J. Chem. Phys.*, 2004, **121**, 2253.
20 M. Roeselová, J. Vieceli, L. X. Dang, B. C. Garrett and D. J. Tobias, *Am. Chem. Soc.*, 2004, **126**.
21 R. Vácha, P. Slavicek, M. Mucha, B. J. Finlayson-Pitts and P. Jungwirth, *J. Phys. Chem. A*, 2004, **108**, 11573.
22 J. Vieceli, M. Roeselová, N. Potter, L. X. Dang, B. C. Garrett and D. J. Tobias, *J. Phys. Chem. B*, 2005, **109**(33), 15876.
23 D. S. Benincasa, P. W. Barber, J. Zhang, W. Hsieh and R. K. Chang, *Appl. Opt.*, 1987, **26**, 1348.
24 C. D. Cappa, K. R. Wilson, B. R. Messer, R. J. Saykally and R. C. Cohen, *Geophys. Res. Lett.*, 2004, **31**, Art. No. L10205.
25 P. Chylek, J. D. Pendleton and R. G. Pinnick, *Appl. Opt.*, 1985, **24**, 3940.
26 C. F. Bohren and D. R. Huffman, *Absorption and Scattering of Light by Small Particles*, Wiley, New York, 1983.
27 P. W. Barber and S. C. Hill, *Light Scattering by Particles: Computational Methods*, World Scientific, Singapore, 1990.
28 A. K. Ray and D. D. Bhanti, *Appl. Opt.*, 1997, **36**, 2663.
29 R. Thurn and W. Kiefer, *Appl. Opt.*, 1985, **24**, 1515.
30 S. Madronich, *J. Geophys. Res.*, 1987, **92**, 9740.
31 A. Ruggaber, R. Dlugi, A. Bott, R. Forkel, H. Herrmann and H.-W. Jacobi, *Atmos. Environ.*, 1997, **31**, 3137.
32 A. Bott and W. Zdunkowski, *J. Opt. Soc. Am. A*, 1987, **4**, 1361.
33 B. J. Finlayson-Pitts and J. N. Pitts, Jr, *Chemistry of the Upper and Lower Atmosphere*, Academic Press, San Diego, 2000.

34 D. J. Griffiths, *Introduction to Electrodynamics*, 3rd edn, Prentice Hall, New Jersey, 1999.
35 A. F. Forziati, D. L. Camin and F. D. Rossini, *J. Res. Natl. Bur. Stand. (U. S.)*, 1950, **45**(5), 406.
36 N. A. Marley, J. S. Gaffney, J. C. Baird, C. A. Blazer, P. J. Drayton and J. E. Frederick, *Aero. Sci. Tech.*, 2001, **34**, 535.
37 S. C. Hill, *Appl. Opt.*, 2003, **42**, 4381.
38 K. E. Lewis, D. M. Golden and G. P. Smith, *J. Am. Chem. Soc.*, 1984, **106**, 3905.
39 D. R. Lide, *CRC Handbook Chemistry and Physics*, 85th edn, CRC Press, Boca Raton, 2004.
40 M. Wrighton, *Chem. Rev.*, 1974, **74**, 401.
41 T. Lian, S. E. Bromberg, M. C. Asplund, H. Yang and C. B. Harris, *J. Phys. Chem.*, 1996, **100**, 11994.
42 J. A. Welch, K. S. Peters and V. Vaida, *J. Phys. Chem.*, 1982, **86**, 1941.
43 J. A. Ganske and R. N. Rosenfeld, *J. Phys. Chem.*, 1989, **93**, 1959.
44 Y. Ishikawa, C. E. Brown, P. A. Hackett and D. M. Rayner, *J. Phys. Chem.*, 1990, **94**, 2404.
45 J. Lelieveld and P. Crutzen, *J. Atmos. Chem.*, 1991, **12**, 229.
46 D. Tobias, P. Jungwirth and M. Parrinello, *J. Chem. Phys.*, 2001, **114**, 7036.
47 L. X. Dang, *J. Phys. Chem. B*, 2002 106, 10338.
48 L. Dang and T. M. Chang, *J. Phys. Chem. B*, 2002, **106**, 235.
49 L. Perera and M. L. Berkowitz, *J. Chem. Phys.*, 1992, **96**, 8288.
50 L. Perera and M. L. Berkowitz, *J. Chem. Phys.*, 1993, **99**, 4222.
51 L. Sremaniak, L. Perera and M. L. Berkowitz, *Chem. Phys. Lett.*, 1994, **218**, 377.
52 S. Stuart and B. J. Berne, *J. Phys. Chem.*, 1996, **100**, 11934.
53 S. Stuart and B. J. Berne, *J. Phys. Chem. A*, 1999, **103**, 10300.
54 M. Wilson and A. Pohorille, *J. Chem. Phys.*, 1991, **95**, 6005.
55 G. M. Hale and M. R. Querry, *Appl. Opt.*, 1973, **12**, 555.
56 A. H. Harvey, J. S. Gallagher and J. M. H. Levelt Sengers, *J. Phys. Chem. Ref. Data*, 1998, **27**, 761.
57 P. Salvador, J. E. Curtis, D. J. Tobias and P. Jungwirth, *Phys. Chem. Chem. Phys.*, 2003, **5**, 3752.
58 L. X. Dang, T.-M. Chang, M. Roeselova, B. C. Garrett and D. J. Tobias, *J. Chem. Phys.*, 2006, **124**, 066101.
59 J. Mack and J. R. Bolton, *J. Photochem. Photobiol., A*, 1999, **128**, 1.
60 Y. Dubowski, A. J. Colussi and M. R. Hoffmann, *J. Phys. Chem. A*, 2001, **105**, 4928.
61 Y. Dubowski, A. L. Colussi, C. Boxe and M. R. Hoffmann, *J. Phys. Chem. A*, 2002, **106**, 6967.
62 J. Thomas, M. Roeselova and D. J. Tobias, in preparation.
63 J. Zhang, D. H. Leach and C. R. K., *Opt. Lett.*, 1988, **13**, 270.
64 N. A. Beach and H. B. Gray, *J. Am. Chem. Soc.*, 1968, **90**, 5713.

